


Dynamical mechanism for generation of arrhythmogenic early afterdepolarizations in cardiac myocytes: Insights from in silico electrophysiological models

Roberto Barrio ^{*}, M. Ángeles Martínez , and Sergio Serrano 

Department of Applied Mathematics and IUMA, Computational Dynamics group, University of Zaragoza, E-50009 Zaragoza, Spain

Esther Pueyo 

I3A, University of Zaragoza, IIS Aragón and CIBER-BBN, E-50018 Zaragoza, Spain

 (Received 12 August 2021; revised 22 June 2022; accepted 10 July 2022; published 3 August 2022)

We analyze the dynamical mechanisms underlying the formation of arrhythmogenic early afterdepolarizations (EADs) in two mathematical models of cardiac cellular electrophysiology: the Sato *et al.* biophysically detailed model of a rabbit ventricular myocyte of dimension 27 and a reduced version of the Luo-Rudy mammalian myocyte model of dimension 3. Based on a comparison of the two models, with detailed bifurcation analysis using spike-counting techniques and continuation methods in the simple model and numerical explorations in the complex model, we locate the point where the first EAD originates in an unstable branch of periodic orbits. These results serve as a basis to propose a conjectured scheme involving a hysteresis mechanism with the creation of alternans and EADs in the unstable branch. This theoretical scheme fits well with electrophysiological experimental data on EAD generation and hysteresis phenomena. Our findings open the door to the development of novel methods for pro-arrhythmia risk prediction related to EAD generation without actual induction of EADs.

DOI: [10.1103/PhysRevE.106.024402](https://doi.org/10.1103/PhysRevE.106.024402)

I. INTRODUCTION

The transmembrane potential (V) of biological cells is the difference in the electrical potential between the inside and the outside of the cell due to the ion concentration gradients between the two sides of the membrane. Electrically excitable cells (muscle cells, neurons, and some secretory cells) have the ability to respond to an applied stimulus by generating an electrical signal that reflects changes in V along time. In the case of cardiac muscle cells, upon being stimulated, they are activated producing an electrical impulse called the action potential (AP). This AP shows different phases. First, there is a rapid increase in the transmembrane voltage (phase 0: depolarization), following which there is a short transient decrease of V (phase 1: transient repolarization). Next, V remains approximately constant (phase 2: plateau phase). Finally, V decreases to the resting membrane potential (phase 3: repolarization) until the cell receives another stimulus. Under some circumstances, secondary voltage depolarizations can appear during phase 2 of the AP, so-called early afterdepolarizations (EADs). In diseases like heart failure and genetic syndromes, EADs have been documented to be an important cause for lethal ventricular arrhythmias [1–3]. Despite large research efforts, further knowledge is still required to gain improved understanding of all possible mechanisms underlying EAD generation.

During the last decades, computational models of cardiac electrical activity have greatly contributed to shed light

on cardiac phenomena, including EADs. Highly detailed complex models with a large number of state variables allow more faithful reproduction of experimental observations and facilitate biophysical interpretation. However, in some cases, in-depth analysis with these complex models can be difficult to perform or it can be prohibitive in terms of computational cost. Simple models, however, allow such analysis and become basic elements to investigate certain phenomena.

Many studies in the literature investigating EADs work with either low-dimensional or high-dimensional models, while only a few of them combine the use of both types of models. In Ref. [4], for example, predictions are obtained using a low-dimensional model, which are subsequently validated using a more complex model. In contrast, here we first obtain our results using a highly detailed model and we explain these results theoretically using a low-dimensional one. Due to the high number of variables and parameters of the 27D Sato model and the impossibility of conducting a theoretical study, we use adapted sweeping numerical techniques to study the dynamical mechanisms of EAD generation and time course, but, if we want to give a theoretical explanation, we need a simpler model, which simulates the behavior (corresponding the EAD appearance) of the more complex model. Thus, the main goals of this work are to provide a theoretical scheme of a possible transition between APs without EADs to APs with EADs and to describe the basic elements involved in that transition.

This paper is organized as follows. In Sec. II we describe briefly the mathematical models used in this study. The results for both models are presented in Sec. III; discussion

^{*}rbarrio@unizar.es; CODY group: <http://cody.unizar.es>.

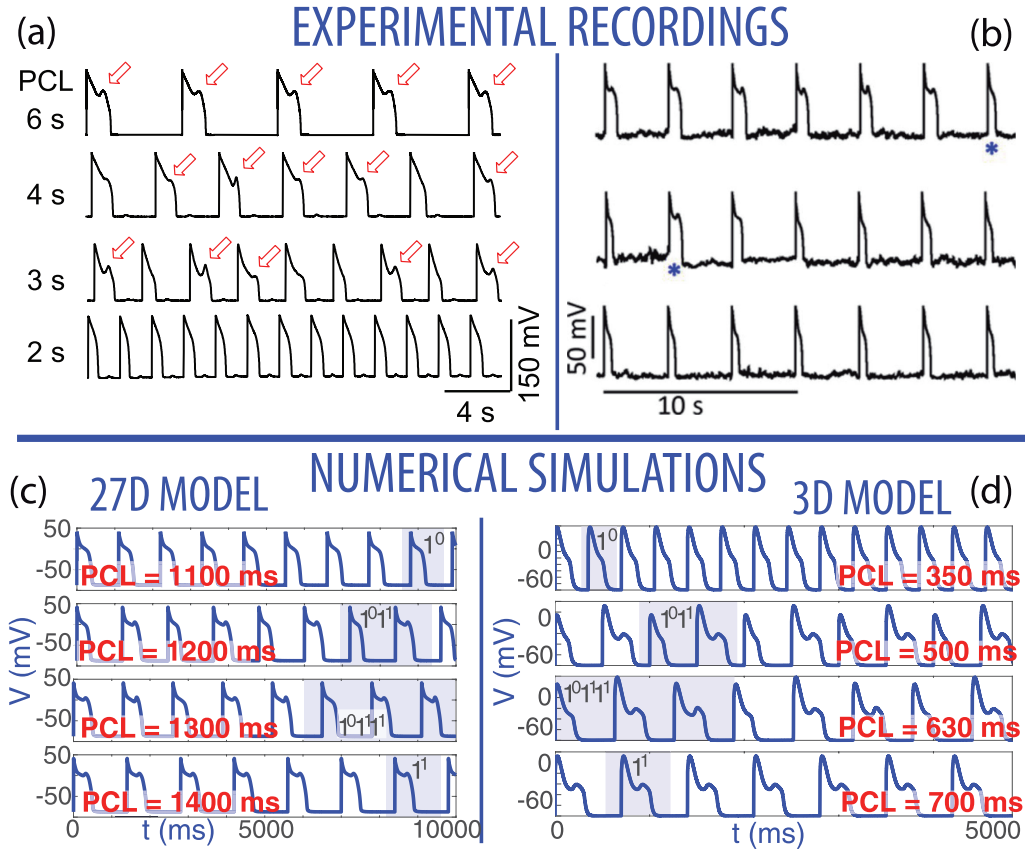


FIG. 1. Experimentally recorded and computationally simulated APs, some of which present EADs. (a) APs from a paced rabbit ventricular myocyte exposed to 1 mM H_2O_2 (taken from Fig. 1(A) of Ref. [3]). Red arrows indicate the presence of an EAD. (b) APs from a rabbit ventricular myocyte under partial block of the rapid delayed rectifier K current (I_{Kr}) with E-4031 (100–200 nmol/L) to prolong AP repolarization (taken from Fig. 1(b) of Ref. [5]). Asterisks denote APs with distinct behavior: in the first sequence, the pointed AP, differently from the rest of APs, does not show an EAD; in the second sequence, the pointed AP is the only one showing an EAD. (c) APs obtained from numerical simulations using the Sato 27D cardiomyocyte model. (d) APs obtained from numerical simulations using the reduced Luo-Rudy 3D cardiomyocyte model. Shadow regions in panels (c) and (d) show one period of the orbit.

are reported in Sec. IV, and finally we summarize our main conclusions in Sec. V.

II. MATHEMATICAL MODELS

We briefly describe the two mathematical models used in this work. As a high-dimensional model, we use the 27D Sato model of the rabbit ventricular myocyte built from the Shannon *et al.* model [6]. This model was first modified by Mahajan *et al.* [7] and later further updated by Sato *et al.* [3] to properly reproduce EADs recorded experimentally, as illustrated in Figure 1. The rate of change of the transmembrane potential (V) is given by

$$C_m \frac{dV}{dt} = -(I_{\text{ion}} + I_{\text{stim}}), \quad (1)$$

where the total ionic current I_{ion} is the sum of nine ionic currents:

$$I_{\text{ion}} = I_{\text{Ca}} + I_{\text{Na}} + I_{\text{Ks}} + I_{\text{Kr}} + I_{\text{K1}} + I_{\text{tos}} + I_{\text{tof}} + I_{\text{NaK}} + I_{\text{NaCa}}.$$

Being I_{Ca} the L-type Ca^{2+} current and I_{Na} the fast sodium current. The potassium current has five components: I_{Ks} and

I_{Kr} correspond to the slow and rapid component (respectively) of the delayed rectifier K^+ current, I_{K1} to the inward rectifier K^+ current and I_{tos} and I_{tof} to the slow and fast component (respectively) of the rapid outward K^+ current. The last two correspond to pump currents. On the one hand the I_{NaK} transports two K^+ ions into the cell in exchange for three Na^+ ions out of the cell and, on the other hand, I_{NaCa} transports three Na^+ ions in and one Ca^{2+} ion out of the cell. An additional stimulus current I_{stim} is included, which in this study is delivered at a constant stimulus period defined by the pacing cycle length (PCL). The complete description of the ionic currents involves 27 ordinary differential equations for the 27 state variables, in which 177 model parameters are used (see Refs. [3,7,8] for full details and equations). The 27D Sato model is a highly detailed model with non-smooth functions, nonlinearities, high dimension and a large number of parameters. The system of 27 ordinary differential equations was solved in C^{++} using an embedded Runge-Kutta formulas [Dormand-Prince RK5(4)] with variable stepsize. The error tolerance was set to 10^{-8} with a minimum time step of 0.002 ms. The complete set of initial conditions for most of the simulations are taken from Ref. [9].

There may be different dynamic mechanisms contributing to the appearance of EADs and multiple ionic currents and concentrations may be involved in EADs generation. Although the aim of this study is not to determine which currents are key in EAD formation, in our previous work, the I_{Ca} current seems to play an important role, as confirmed by the fact that inhibiting this current, even to only modest extents, precluded EAD formation. This agrees with other works where the relevance of the I_{Ca} current is shown [10–12] even if not being the only factor. Here we focus on potential dynamic mechanisms that can induce EADs.

In our analysis of this model, we use PCL and g_{Ks} (peak I_{Ks} conductance) as bifurcation parameters. PCL has been shown to play an important role in the dynamics of this model [9,13] and there are many studies showing the importance of the potassium current in the genesis of early afterdepolarizations in cardiac cells [14]. See Ref. [9] for a more detailed study of the dynamics of the Sato model.

As a low-dimensional model, we use a reduced 3D version of the Luo-Rudy mammalian cardiac cell model (LR91) [13,15]. The model includes two ionic currents and it is defined by three ODEs:

$$\begin{aligned} C_m \frac{dV}{dt} &= -(I_{Ca} + I_K + I_{stim}), \\ \frac{df}{dt} &= \frac{f_\infty(V) - f}{\tau_f}, \\ \frac{dx}{dt} &= \frac{x_\infty(V) - x}{\tau_x}. \end{aligned} \quad (2)$$

Also in this case, I_{stim} is an external stimulus current of period PCL. Here, we define I_{stim} to have an amplitude of $-40 \mu\text{A}/\text{cm}^2$ and duration of 1 ms for the two analyzed models. The ionic currents I_{Ca} and I_K are defined by $I_{Ca} = G_{Ca}d_\infty(V)f(V - E_{Ca})$ and $I_K = G_Kx(V - E_K)$. The steady-state functions $f_\infty(V)$, $x_\infty(V)$, and $d_\infty(V)$ are given by standard Boltzmann functions. For this model, we investigate the impact on cellular electrical activity of changes in two parameters: PCL and G_K (the conductance of the I_K current).

From a mathematical point of view, this is a fast-slow dynamical system with multitime-scale phenomena [16]. The first fast-slow decomposition of this system, considering 1-slow–2-fast variables [17], showed the presence of a subcritical Poincaré-Andronov-Hopf bifurcation in the fast subsystem. This approach has been successfully used in a variety of cardiac studies to investigate the causes for the presence or absence of EADs. More recently, some studies have shown that this fast-slow decomposition may not provide a satisfactory explanation for certain EAD generation analysis. In Ref. [18] another paradigm was introduced using a 1-fast–2-slow decomposition that has proved to be more suitable. The reduced 3D version of the LR model with a 1-fast–2-slow decomposition [18–20] provides further insight into the facilitation or preclusion of EADs as a function of the pacing frequency or pharmacological interventions.

Figures 1(a) and 1(b) present experimental APs recorded in rabbit ventricular myocytes at different values of PCL under different interventions [3,5]. As can be observed from the figure, some of these experimental APs present EADs. This behavior is reproduced by the two models analyzed in

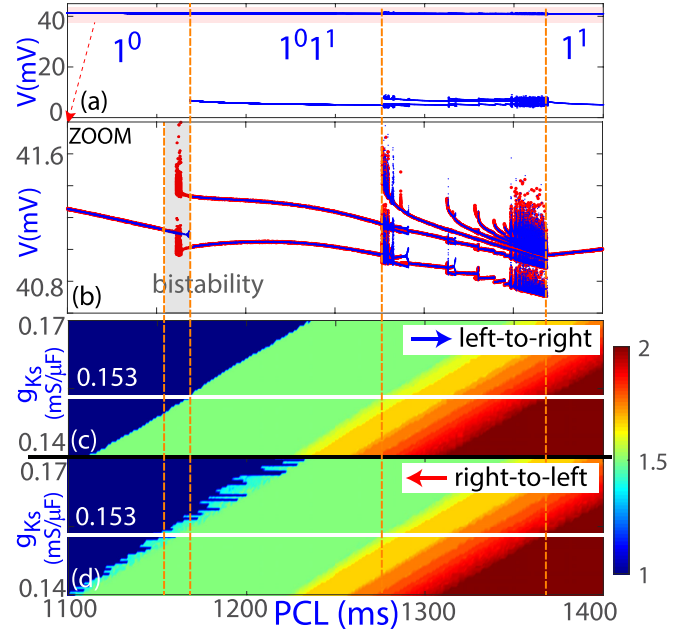


FIG. 2. Numerical analysis of the Sato 27D model. (a) Bifurcation diagram obtained by varying PCL. The blue points on the top part of the bifurcation diagram correspond to the AP peaks (≈ 41 mV) and those on the bottom part correspond to the EAD peaks (≈ 8 mV). Symbolic sequences 1^0 , $1^0 1^1$, and 1^1 denote periodic orbits with the following characteristics: without EAD; one AP without EAD and one AP with EAD; and all APs with EAD, respectively. (b) Zoomed in version of the top part in panel (a) to show the structure of the bifurcation diagram corresponding to the AP peaks. The points in blue show the diagram obtained when varying PCL from left to right (i.e., starting each numerical integration from the final conditions of the previous PCL value) and the points in red show the diagram for varying PCL from right to left. Intervals with dots of different colors that do not overlap indicate bistability. (c, d) Biparametric bifurcation diagrams considering PCL and g_{Ks} as free parameters. Color code corresponds to the ratio between the number of voltage peaks and the number of APs. The horizontal white line is associated with the default value of $g_{Ks} = 0.153$ mS/ μF in the Sato 27D model, which was used to obtain the bifurcation diagrams of panels (a) and (b).

this study when varying PCL. This is shown in Fig. 1(c) for the Sato 27D cardiomyocyte model and in Fig. 1(d) for the reduced 3D version of the Luo-Rudy cardiomyocyte model.

III. RESULTS

From the simulated APs presented in Fig. 1 using the two mathematical models considered in this study, it can be seen that, when varying PCL, there are transitions from APs without EADs to some APs having EADs to all APs presenting EADs. The first question in this study is whether the evolution of the two models is comparable in the sense that they undergo similar transitions. To answer this question, we focus on the results shown in Figs. 2 and 3. Figure 2 presents the simulation results obtained using the Sato 27D model, while Fig. 3 presents those corresponding to the reduced Luo-Rudy 3D model. The top panels of these two figures [Figs. 2(a), 2(b), and 3(a)] show the bifurcation diagram obtained by

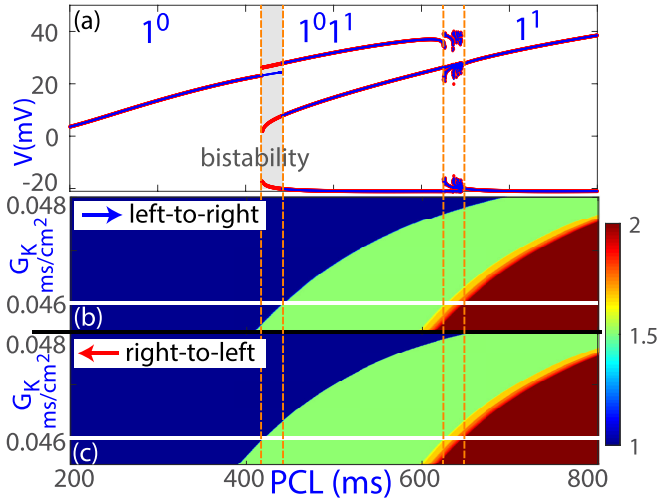


FIG. 3. Numerical analysis of the reduced Luo-Rudy 3D model. (a) Bifurcation diagram obtained by varying PCL. The blue points show the diagram obtained when varying PCL from left to right and the points in red show the diagram for varying PCL from right to left. (b, c) Biparametric bifurcation diagrams considering PCL and G_K as free parameters. Color code corresponds to the ratio between the number of voltage peaks and the number of APs. The horizontal white line is associated with the default value of $G_K = 0.046$ mS/cm² in the reduced Luo-Rudy 3D model, which was used to obtain the bifurcation diagram of panel (a).

setting all the parameters of the models to their default values and only varying the value of PCL. In both cases, PCL is varied along an interval whose left end has a single periodic attractor with a single AP without EAD, sequence 1^0 , while its right end has a single periodic attractor with an AP that always presents an EAD, sequence 1^1 . Here, we use the Farey sequence notation L^s , taken from the mixed-mode oscillations (MMO) literature [16], to characterize the periodic orbits with large (L) and short (s) oscillations. For intermediate values of PCL, different subintervals can be observed where the periodic attractor has several APs, one of them without EAD and the rest of them with EAD. The number of APs with EAD in each of these subintervals grows with the PCL value. Separating these subintervals, transition regions characterized by the existence of bistability can be appreciated. Figure 2(b) is a magnification of the upper peaks of the APs in Fig. 2(a) to facilitate visualization of the internal structure. In these bifurcation diagrams, two colors are used to represent the continuation in the two possible directions, increasing PCL (blue) and decreasing PCL (red). Thus, the existence of points with different colors indicates the coexistence of attractors and, therefore, bistability.

To study the evolution of the model dynamics more globally, a two-parameter bifurcation diagram is represented in the two bottom panels of Figs. 2 and 3. In addition to varying PCL, in this case the parameter g_{Ks} for the Sato 27D model and the parameter G_K for the Luo-Rudy 3D model are allowed to vary as well. The white line segment in each of these panels indicates the default value of g_{Ks} or G_K used for the bifurcation diagrams of the upper panels. Different colors are used to represent different values of the ratio between the

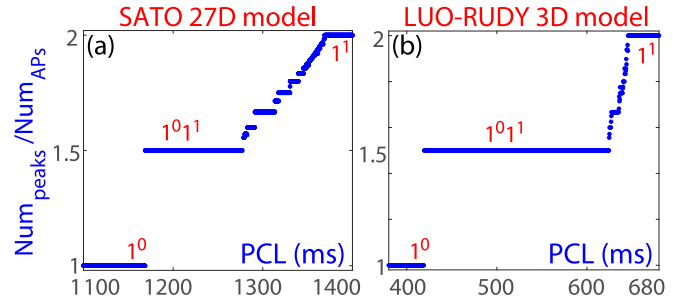


FIG. 4. Cardiac Devil's staircase for (a) Sato 27D model and (b) reduced Luo-Rudy 3D model. The figures show the ratio between the number of voltage peaks and the number of APs for the selected lines in Figs. 2 and 3. Although the sizes of the steps are not the same in the two models, the coincidence in the structure is evident.

number of voltage peaks (accounting for both AP peaks and EAD peaks) and the number of APs. Thus, this ratio takes a value of 1 for the sequence 1^0 and a value of 2 for the sequence 1^1 . For both models, the two-parameter bifurcation diagrams, obtained by additionally allowing the second parameter to vary around its default value, present similar behavior to the previously described one-parameter bifurcation diagrams. In both cases, increasing the potassium conductance delays the transition. In any case, the same color bands representative of ratios with the same values are detectable in the two models. Furthermore, with the biparametric bifurcation diagrams, we see the same structure by fixing the PCL and varying the value of the potassium conductance. From these results, it can be concluded that the evolution of the model dynamics along the analyzed PCL intervals is overall the same for the Sato and the reduced Luo-Rudy models, although the scales for voltage and PCL are different.

The parallelism in the evolution of the two mathematical models is also illustrated in Fig. 4, where the ratio between the number of voltage peaks and the number of APs for the selected lines in Figs. 2 and 3 is shown. This ratio shows an ascending staircase-like behavior when varying PCL. The values taken by the ratio range from 1 (sequence 1^0) to 2 (sequence 1^1) with intermediate steps presenting lengths of variable size corresponding to the transition regions shown in the bifurcation diagrams. This ratio staircase is called *cardiac Devil's staircase* [9,21]. From Fig. 4, and the previous ones, we suggest that, in the investigated parametric plane, the transition characteristics for the Sato 27D and reduced Luo-Rudy 3D models are similar.

IV. DISCUSSION

In the following, the relevant question on how to connect the two coexisting stable orbits (bistability) shown in the transition regions of Figs. 2 and 3 is addressed. In particular, we focus on the first of the transition regions from APs without EADs (sequence 1^0) to one every two APs having EADs (sequence $1^0 1^1$). Results are presented in Figs. 5 and 6. From Fig. 5, showing results for the Sato 27D model, it is possible to observe that the orbit without EADs experiences a process of generation of alternans via a torus bifurcation. Although options alternative to the torus bifurcation would be possible,

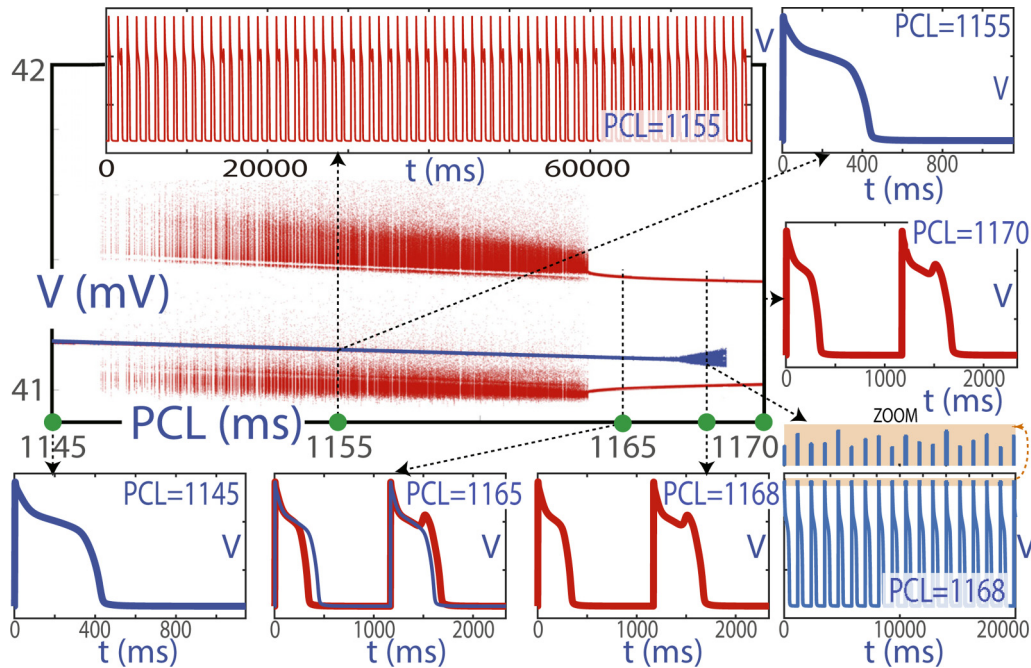


FIG. 5. Central panel shows a magnification of the bifurcation diagram of Fig 2(b) in the EAD transition region between periodic orbits 1^0 and $1^0 1^1$ for the Sato 27D model. Blue points and red points correspond to different attractors. Green dots and arrows relate PCL values to the corresponding voltage time series shown in the surrounding panels. For PCL values in which there is bistability, the voltage time series of the two attractors (each in the corresponding color) are shown.

in this case the bifurcation diagram and the voltage time series of the blue orbit for $PCL = 1168$ points out to that bifurcation. From the same figure, the stable family of orbits with EADs (red points) can be seen to end in a noisy area when PCL is decreased. A set of voltage time series is shown in the figure for the orbits of both families illustrating standard orbits, alternans, chaotic orbits and torus behavior. From the bifurcation diagram in the central panel of Fig. 5, one can conjecture a hysteresis phenomenon giving rise to the observed bistability that is detected in biological experiments too [5,22,23]. The two branches in the panel would be connected, but this is not possible to be evaluated using the Sato 27D model. Thus, we conduct a more detailed analysis of the same transition from non-EADs to EADs using the reduced Luo-Rudy 3D model, as shown in Fig. 6. In this case, the complete families of periodic orbits (stable and unstable ones) are obtained using the AUTO continuation software [24,25]. The use of simple iterated map models [26] has recently allowed the analysis of bifurcations involved in phenomena caused by feedback between a number of magnitudes. In our case, continuation techniques applied to the reduced Luo-Rudy 3D model allow visualizing the complete evolution of the different periodic orbits and facilitate linking them to the behavior observed with more complex models and/or experiments.

The role of different dynamical mechanisms have been studied in previous works. For instance, the generation of alternans and EADs via period-doubling and torus bifurcations have been studied in Refs. [11,12]. The link with period-doubling bifurcations and bistability is shown in Ref. [27]. The existence of hysteresis phenomenon has been illustrated in numerical models and in experiments [22,23]. References [4,10] relate the Hopf and homoclinic bifurcations of the

1-slow-2-fast decomposition with some experiments showing changes before and after EAD generation. In particular, in Ref. [10] the influence of different currents in the EAD generation is reported. In Ref. [28], the role of alternans in the generation of lethal cardiac arrhythmias and sudden cardiac death is described. The change from 1-slow-2-fast to 1-fast-2-slow decomposition was used in Ref. [18] and later in Refs. [19,20] to analyze the creation of new EADs via singular perturbation theory.

In this study, we combine different dynamical mechanisms to provide a complete scheme that explains the steps of a possible route to EAD generation. This scheme locates the exact position of the EAD generation point that is placed in an unstable branch of periodic orbits of a hysteresis loop. Note that, up to our knowledge, the exact location of the EAD generation point has not been reported in literature where mechanisms underlying EAD generation have been described but not the EAD location point. To obtain this position, several numerical techniques, as continuation and spike-adding methods, are required to be used in conjunction. Here, we explain the sudden change from normal beats to EADs. We describe it as an “invisible” phenomenon because the change is in the unstable coexisting periodic orbits and this cannot be observed in experiments where only the stable branches can be seen. This invisible change is related to the recently reported concept of tipping points [29], where a sudden change between two clearly different behaviors is observed, but a smooth change in the unstable invariants occurs.

The top plot of Fig. 6 shows the bifurcation diagram plotting the voltage peaks of the different periodic orbits obtained using the continuation software. The central panel shows the same bifurcation diagram but plotting L_2 norm of these

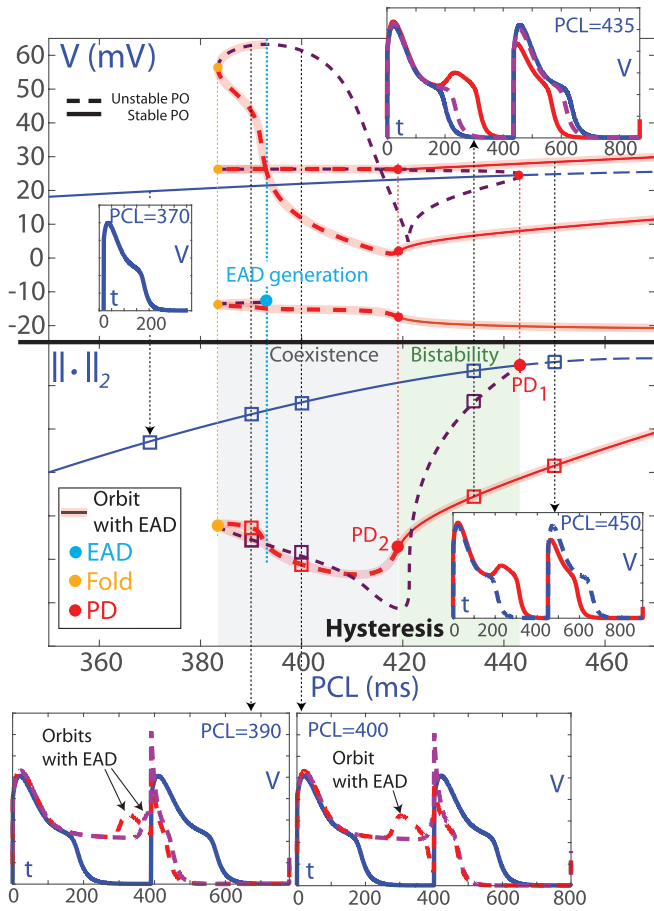


FIG. 6. Top panel shows a magnification of the bifurcation diagram of Fig 3(a) in the EAD transition region between periodic orbits 1^0 and $1^0 1^1$ for the reduced Luo-Rudy 3D model. This bifurcation diagram has been completed with the unstable branches calculated by the AUTO continuation software. The main bifurcations [period-doubling (PD) and fold (of limit cycles)] that influence the stability of the periodic orbits are marked with red and yellow dots. The blue dot corresponding to the EAD generation point is located where a low voltage peak is created in the unstable branch. The central panel shows the above bifurcation diagram, but for the L_2 norm of the periodic orbits rather than the voltage peaks of those orbits. The two stable branches can be seen to be connected by an unstable branch that evolves continuously from one to the other. The bistability and coexistence regions have been marked in green and grey, respectively. The voltage time series of the points marked with small colored squares are also shown and each of the curves in the time traces correspond to the different branches, according to the type of line.

periodic orbits. Branches with unstable periodic orbits are dashed color lines, while the solid color curves represent the branches with stable periodic orbits. Besides, some relevant bifurcation points are located: the period-doubling (red PD_1) point leading to the generation of alternans in this model; the (red PD_2) point leading to destabilization of the red family and creation of some chaotic behaviors; and the fold (yellow) point where the periodic orbit family generates the hysteresis phenomenon with different coexistence orbits, with or without bistability. Note that this hysteresis phenomenon also gives

rise to so-called tipping points [29] in cardiac dynamics that mark the point of sudden onset of EADs in experiments. Furthermore, from the top plot of the figure it is possible to identify where the EAD is created (denoted by the light blue dot point and with the dashed blue vertical line) in the periodic family, which corresponds to the unstable part of the hysteresis. Since the voltage peaks are shown in the panel, the appearance of a new peak of a lower value indicates the creation of the EAD. This can be seen to be located at the origin of the lower voltage branch. To make it easier to identify the unstable part where an EAD is found, the corresponding dashed curves have a thick transparent red line below them. This hysteresis phenomenon is more evident in the central plot using the L_2 norm. If we start on the blue stable branch 1^0 with $PCL = 350$ and we increase PCL until reaching PD_1 , that branch becomes unstable. We now leave the blue branch to continue along the purple branch (decreasing PCL value). Initially, this branch represents periodic orbits with alternans $1^0 1^0$, i.e., no EAD, until the branch meets the EAD generation value (dashed blue vertical line), where the orbit becomes $1^1 1^0$ and presents one AP with EAD and another AP without EAD. From that moment on, the curve will have a transparent red background to mark the existence of EAD. Continuing along that branch, a fold is reached where another branch merges with this one. The new unstable (dashed red) branch gets to PD_2 where it becomes stable. The voltage time series of the existing attractors for different PCL values are also shown in Fig. 6 to help visualize their evolution throughout the transition. The lower plots show the time series of three periodic orbits on vertical sections inside the hysteresis region of coexistence, where the EAD is created. The picture on the right side of the EAD generation point is before the generation of EAD for the purple unstable branch, and so only one unstable periodic orbit has EAD (red branch). On the left side of the EAD generation point the unstable periodic orbit corresponding to the purple branch has an extra spike and, consequently, an EAD has appeared. Note that, as the plateau phase (phase 2) of the AP has increased enough, the unstable periodic orbits in this area have an extra AP and the EAD appears near it. One theoretical explanation of this increment of the plateau phase of the AP is related to the mechanism of creation of EADs via “canards” [16] as shown in Refs. [18–20]. This mechanism is theoretically based on the assumption that the reduced model is a 2-slow–1-fast slow-fast model, rather than a 1-slow–2-fast slow-fast model as considered in Ref. [17]. In that case, the existence of a Hopf bifurcation in the fast subsystem explained theoretically the appearance of EADs, but, as shown in Ref. [18], the 1-slow–2-fast model is not the most suitable model in some cases, and the 2-slow–1-fast one provides a more suitable framework. In any case, in both situations, the location of the EAD generation point remained to be elucidated. That hitherto unknown location is the one we have detected using continuation in the 3D model. This is shown in Fig. 6, where we can see how that point is in the unstable branch of the hysteresis coexistence region. Detecting the origin of the EADs is not otherwise possible, since it is located in the unstable branch. Therefore, such origin is “invisible” experimentally. However, the hysteresis, created in the fold, in which both attractors (with and without EADs) coexist, is observable and its effects are visible, both in the

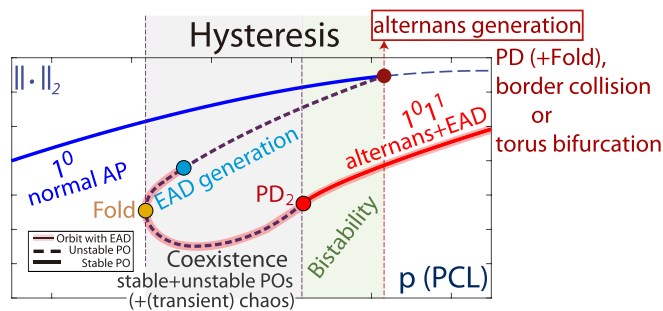


FIG. 7. Conjectured theoretical bifurcation scheme of a possible mechanism for the development of the first EADs. This scheme shows the minimum required elements, in view of the numerical results, for the transition between the periodic orbits of sequence 1^0 and of sequence $1^0 1^1$.

reduced and extended models (see Figs. 2 and 3) and in the experiments. Furthermore, the appearance of alternans in the 1^0 branch is an indicator in this case of the region where we can easily end up in the 1^1 branch. In fact, the generation of alternans leads to one AP evolving toward the appearance of an EAD in it, and the other AP not having it.

Summarizing, in both the Sato 27D and the reduced Luo-Rudy 3D models, it can be observed that the periodic orbit without EAD experiences a bifurcation (torus bifurcation or period-doubling bifurcation) that generates the appearance of alternans. Subsequently, the family with alternans evolves, creating a hysteresis and some of them begin to experience EADs in the unstable branch. This alternation between an AP without EAD and an AP with EAD leads to the periodic sequence $1^0 1^1$ and the change from non-EADs to EADs, with a connection via an unstable branch of periodic orbits.

V. CONCLUSIONS

Taking into account all the presented results, we conjecture a theoretical scheme that explains a possible mechanism for the generation of the first EADs in APs. This mechanism would apply to both experimentally recorded and computationally simulated APs, as the ones shown in Fig. 1. The proposed theoretical scheme with the basic ingredients (although there may be more) is shown in Fig. 7: alternans generation [30], fold bifurcation (giving rise to a hysteresis phenomenon), EAD generation in the unstable branch, fold

bifurcation and period-doubling ending the hysteresis and generating some chaotic behavior (more options are possible, such as a subcritical period-doubling). The generation of alternans can be caused by several bifurcations like period-doubling, border collision [31] or torus bifurcation, but, in any case, it seems that prior generation of alternans is required for the subsequent appearance of the first EAD, very recently related to the canard phenomenon [18–20]. Note that our results using the link of complex and simple models and the use of continuation and sweeping techniques allow us to locate the EAD generation point in the unstable branch of the hysteresis loop connecting both stable branches (one without and one with EAD).

Our findings open the door to pro-arrhythmia risk prediction related to the appearance of EADs before these EADs actually appear. Also, our outcomes may prove helpful for the investigation of the mechanisms lying behind the observed EAD patterns and the design of related interventions. Although such mechanisms may involve highly varied ionic sources and, thus, comprehensive research should be conducted to elucidate them, the I_{Ca} current appears to be an important contributor in the investigated models. Indeed, inhibition of this current completely abolished EADs in both the Sato 27D and the reduced Luo-Rudy 3D models, while manipulations of other currents like the sodium-calcium exchanger in the detailed Sato model had less relevant effects. Strategies directed to modulate specific properties of the I_{Ca} current so as to prevent EAD generation while preserving excitation-contraction coupling could be tested on the basis of the present research.

ACKNOWLEDGMENTS

The authors thank Dr. S. Otte for kindly sharing his code of the Sato cardiomyocyte model with us. R.B., M.A.M., and S.S. have been supported by the European Social Fund (EU) and Aragón Government (Grant No. LMP124-18 and Group E24-17R) and by the European Social Fund (EU) and Spanish Ministry of Science and Innovation (Grants No. PGC2018-096026-B-I00 and No. PID2021-122961NB-I00). E.P. has been supported by the European Research Council (Grant No. 638284) and European Social Fund (EU) and Aragón Government (Grant No. LMP94-21 and Group T39-20R). M.A.M., E.P., and S.S. have also been supported by the Spanish Ministry of Science and Innovation (Grant No. PID2019-105674RB-I00).

- [1] C. Antzelevitch and S. Sicouri, Clinical relevance of cardiac arrhythmias generated by afterdepolarizations. Role of M cells in the generation of U waves, triggered activity and torsade de pointes, *J. Am. Coll. Cardiol.* **23**, 259 (1994).
- [2] R. B. Huffaker, J. N. Weiss, and B. Kogan, Effects of early afterdepolarizations on reentry in cardiac tissue: A simulation study, *Am. J. Physiol.: Heart Circ. Physiol.* **292**, H3089 (2007).
- [3] D. Sato, L.-H. Xie, A. A. Sovari, D. X. Tran, N. Morita, F. Xie, H. Karagueuzian, A. Garfinkel, J. N. Weiss, and Z. Qu, Synchronization of chaotic early afterdepolarizations in the genesis of cardiac arrhythmias, *Proc. Natl. Acad. Sci. USA* **106**, 2983 (2009).
- [4] X. Huang, Z. Song, and Z. Qu, Determinants of early afterdepolarization properties in ventricular myocyte models, *PLoS Comput. Biol.* **14**, e1006382 (2018).
- [5] Y. Xie, Z. Liao, E. Grandi, Y. Shiferaw, and D. M. Bers, Slow $[Na]_i$ changes and positive feedback between membrane potential and $[Ca]_i$ underlie intermittent early afterdepolarizations and arrhythmias, *Circ. Arrhythm. Electrophysiol.* **8**, 1472 (2015).

- [6] T. R. Shannon, F. Wang, J. Puglisi, C. Weber, and D. M. Bers, A mathematical treatment of integrated Ca dynamics within the ventricular myocyte, *Biophys. J.* **87**, 3351 (2004).
- [7] A. Mahajan, Y. Shiferaw, D. Sato, A. Baher, R. Olcese, L.-H. Xie, M.-J. Yang, P.-S. Chen, J. G. Restrepo, A. Karma, A. Garfinkel, Z. Qu, and J. N. Weiss, A rabbit ventricular action potential model replicating cardiac dynamics at rapid heart rates, *Biophys. J.* **94**, 392 (2008).
- [8] S. Otte, S. Berg, S. Luther, and U. Parlitz, Bifurcations, chaos, and sensitivity to parameter variations in the Sato cardiac cell model, *Commun. Nonlinear Sci. Numer. Simulat.* **37**, 265 (2016).
- [9] R. Barrio, M. A. Martínez, E. Pueyo, and S. Serrano, Dynamical analysis of early afterdepolarization patterns in a biophysically detailed cardiac model, *Chaos: An Int. J. Nonlinear Sci.* **31**, 073137 (2021).
- [10] Z. Qu, L.-H. Xie, R. Olcese, H. Karagueuzian, P.-S. Chen, A. Garfinkel, and J. Weiss, Early afterdepolarizations in cardiac myocytes: Beyond reduced repolarization reserve., *Cardiovascular research* **99**, 6 (2013).
- [11] F. Grégoire-Lacoste, V. Jacquemet, and A. Vinet, Bifurcations, sustained oscillations and torus bursting involving ionic concentrations dynamics in a canine atrial cell model, *Math. Biosci.* **250**, 10 (2014).
- [12] Y. Kurata, K. Tsumoto, K. Hayashi, I. Hisatome, M. Tanida, Y. Kuda, and T. Shibamoto, Dynamical mechanisms of phase-2 early afterdepolarizations in human ventricular myocytes: Insights from bifurcation analyses of two mathematical models, *Am. J. Physiol.: Heart Circ. Physiol.* **312**, H106 (2017).
- [13] D. Sato, L.-H. Xie, T. P. Nguyen, J. N. Weiss, and Z. Qu, Irregularly appearing early afterdepolarizations in cardiac myocytes: Random fluctuations or dynamical chaos? *Biophys. J.* **99**, 765 (2010).
- [14] Z. Zhao, Y. Xie, H. Wen, D. Xiao, C. Allen, N. Fefelova, W. Dun, P. Boyden, Z. Qu, and L. Xie, Role of the transient outward potassium current in the genesis of early afterdepolarizations in cardiac cells, *Cardiovasc. Res.* **95**, 308 (2012).
- [15] C. Luo and Y. Rudy, A model of the ventricular cardiac action potential. depolarization, repolarization, and their interaction, *Circ. Res.* **68**, 1501 (1991).
- [16] M. Desroches, J. Guckenheimer, B. Krauskopf, C. Kuehn, H. M. Osinga, and M. Wechselberger, Mixed-mode oscillations with multiple time scales, *SIAM Rev.* **54**, 211 (2012).
- [17] D. X. Tran, D. Sato, A. Yochelis, J. N. Weiss, A. Garfinkel, and Z. Qu, Bifurcation and chaos in a model of cardiac early afterdepolarizations, *Phys. Rev. Lett.* **102**, 258103 (2009).
- [18] P. Kügler, A. H. Erhardt, and M. Bulelzi, Early afterdepolarizations in cardiac action potentials as mixed mode oscillations due to a folded node singularity, *PLoS One* **13**, e0209498 (2018).
- [19] R. Barrio, M. A. Martínez, L. Pérez, and E. Pueyo, Bifurcations and slow-fast analysis in a cardiac cell model for investigation of early afterdepolarizations, *Mathematics* **8**, 880 (2020).
- [20] T. Vo and R. Bertram, Why pacing frequency affects the production of early afterdepolarizations in cardiomyocytes: An explanation revealed by slow-fast analysis of a minimal model, *Phys. Rev. E* **99**, 052205 (2019).
- [21] P. Bak, The Devil's staircase, *Phys. Today* **39**, 38 (1986).
- [22] A. R. Yehia, D. Jeandupeux, F. Alonso, and M. R. Guevara, Hysteresis and bistability in the direct transition from 1:1 to 2:1 rhythm in periodically driven single ventricular cells, *Chaos* **9**, 916 (1999).
- [23] K. Tsumoto, Y. Kurata, K. Furutani, and Y. Kurachi, Hysteretic dynamics of multi-stable early afterdepolarisations with repolarisation reserve attenuation: A potential dynamical mechanism for cardiac arrhythmias, *Sci. Rep.* **7**, 10771 (2017).
- [24] E. Doedel, AUTO: A program for the automatic bifurcation analysis of autonomous systems, in *Proceedings of the 10th Manitoba Conference on Numerical Mathematics and Computing, Vol. 1 (Winnipeg, Man., 1980)*, Vol. 30 (1981), pp. 265–284.
- [25] E. J. Doedel, R. Paffenroth, A. R. Champneys, T. F. Fairgrieve, Y. A. Kuznetsov, B. E. Oldeman, B. Sandstede, and X. J. Wang, Auto2000, <http://cmvl.cs.concordia.ca/auto>.
- [26] J. Landaw and Z. Qu, Bifurcations caused by feedback between voltage and intracellular ion concentrations in ventricular myocytes, *Phys. Rev. Lett.* **123**, 218101 (2019).
- [27] P. Kügler, M. Bulelzi, and A. H. Erhardt, Period doubling cascades of limit cycles in cardiac action potential models as precursors to chaotic early afterdepolarizations, *BMC Syst. Biol.* **11**, 42 (2017).
- [28] Z. Qu, Y. Xie, A. Garfinkel, and J. Weiss, T-wave alternans and arrhythmogenesis in cardiac diseases, *Front. Phys.* **1**, 154 (2010).
- [29] M. Scheffer, S. R. Carpenter, T. M. Lenton, J. Bascompte, W. Brock, V. Dakos, J. van de Koppel, I. A. van de Leemput, S. A. Levin, E. H. van Nes, M. Pascual, and J. Vandermeer, Anticipating critical transitions, *Science* **338**, 344 (2012).
- [30] E. Pueyo, A. Corrias, L. Virág, N. Jost, T. Szél, A. Varró, N. Szentandrásy, P. P. Nánási, K. Burrage, and B. Rodríguez, A multiscale investigation of repolarization variability and its role in cardiac arrhythmogenesis, *Biophys. J.* **101**, 2892 (2011).
- [31] C. M. Berger, X. Zhao, D. G. Schaeffer, H. M. Dobrovolny, W. Krassowska, and D. J. Gauthier, Period-doubling bifurcation to alternans in paced cardiac tissue: Crossover from smooth to border-collision characteristics, *Phys. Rev. Lett.* **99**, 058101 (2007).